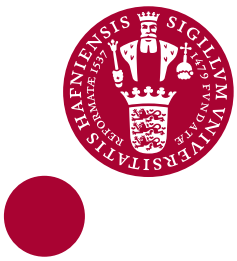

Pb-Pb chronometry and the early Solar System

Connelly, James; Bollard, Jean Francois André; Bizzarro, Martin

Published in:
Geochimica et Cosmochimica Acta

DOI:
10.1016/j.gca.2016.10.044

Publication date:
2017

Document version
Publisher's PDF, also known as Version of record

Available online at www.sciencedirect.com

ScienceDirect

Geochimica et Cosmochimica Acta 201 (2017) 345–363

Geochimica et Cosmochimica Acta

www.elsevier.com/locate/gca

Pb–Pb chronometry and the early Solar System

J.N. Connelly *, J. Bollard, M. Bizzarro

Centre for Star and Planet Formation, Natural History Museum of Denmark, University of Copenhagen, Copenhagen, Denmark

Received 23 March 2016; accepted in revised form 27 October 2016; available online 4 November 2016

Abstract

Of the long-lived chronometric systems, only the dual decay of ^{238}U and ^{235}U to ^{206}Pb and ^{207}Pb, respectively, have appropriate half-lives to resolve the ages of meteorites and their components formed in the first 5 Myr of the Solar System. This paper reviews the theory and methods behind this chronometer, offers criteria to critically evaluate Pb–Pb ages and presents a summary of the current state and immediate future of the chronometry of the early Solar System. We recognize that there is some debate over the age of the Solar System, but conclude that an age of 4567.30 ± 0.16 Ma based on four CAIs dated individually by the same method in two different laboratories is presently the best constrained published value. We further conclude that nebular chondrules dated by the Pb–Pb method require that they formed contemporaneously with CAIs and continued to form for at least ~4 Myr, a conclusion that implies heterogeneous distribution of the short-lived ^{26}Al nuclide in the protoplanetary disk. Planetesimals were already forming by ~1 Myr after CAI formation, consistent with their growth predominantly through the accretion of chondrules. Nebular chondrule formation was completed by ~5 Myr after CAI formation when the impact-generated Cba chondrules formed after the disk was cleared of gas and dust. We note that the absolute age of the Solar System or any single early Solar System object is not fundamental to any significant scientific question and that it is important only to know the correct relative ages of objects being used to piece together the formation history of the Solar System. As such, we point out the risks inherent in comparing Pb–Pb ages produced by different approaches in different laboratories at the level of the internal errors of individual ages. Until a cross-calibration exercise using synthetic and natural standards establishes the reproducibility between laboratories, only ages from a single laboratory, or between laboratories having demonstrated concordance, can provide a reliable relative chronometric framework for the formation and evolution of the early Solar System.

Keywords: U-Pb chronology; Early Solar System; Meteorites; Calcium-aluminum inclusions; Chondrules

1. INTRODUCTION

The first three to five million years of our Solar System's existence spans the initial collapse of a giant molecular cloud containing dust and gas from earlier generations of stars, formation of a protoplanetary disk around the nascent Sun and the emergence of planetesimals and planets (Kleine et al., 2009; Krot et al., 2009; Connelly et al., 2012). Understanding this highly-energetic and dynamic early stage of planetary evolution requires chronometric information with sufficient resolution to place the fragmental record preserved in meteorites into the correct temporal framework. Whereas the decay of short-lived radionuclides such as ^{26}Al inherited from the molecular cloud have the best theoretical potential to yield high-fidelity chronometric records, these decay systems all critically depend on the disputed assumption of homogeneous distribution of the parent nuclide (Larsen et al., 2011; Kita et al., 2013; Schiller et al., 2015; Van Kooten et al., 2016). As such, only the dual U–Pb decay system has the capacity to date individual samples by an assumption free method with sufficiently high

* Corresponding author.
E-mail address: connelly@snm.ku.dk (J.N. Connelly).

http://dx.doi.org/10.1016/j.gca.2016.10.044
0016-7037/

resolution to unravel the timing of meteoritic components formed in the first three to five million years of our Solar System's history (Amelin et al., 2009). This paper reviews the theoretical aspects of the U–Pb and derivative Pb–Pb chronometric systems, analytical methods, ideal and non-ideal applications, a summary of the current chronology of the early Solar System and, finally, future directions.

2. URANIUM-CORRECTED PB–PB DATING

2.1. The U–Pb decay system

Lead has four naturally occurring isotopes of ^{204}Pb, ^{206}Pb, ^{207}Pb and ^{208}Pb that were inherited from the molecular cloud in relative abundances of 1: 9.307: 10.294: 29.476 as measured in troilite from the Type IAB Canyon Diablo iron meteorite (Tatsumoto et al., 1973). The latter three Pb isotopes have increased in abundances through the radioactive decay of ^{238}U, ^{235}U and ^{232}Th, respectively, with half-lives (Table 1) that make the U–Pb decay systems ideally suited for dating materials formed in the first 5 Myr of the Solar System. Only ^{204}Pb preserves its primordial abundances such that the radiogenic ingrowth of Pb isotopes is most conveniently expressed as ^{206}Pb/^{204}Pb, ^{207}Pb/^{204}Pb and ^{208}Pb/^{204}Pb ratios that evolved according to the equation:

$$\left(\frac{^{20x}\mathrm{Pb}}{^{204}\mathrm{Pb}}\right)_{\mathrm{today}} = \left(\frac{^{20x}\mathrm{Pb}}{^{204}\mathrm{Pb}}\right)_{t_0} + \left(\frac{^{23z}\mathrm{U},^{232}\mathrm{Th}}{^{204}\mathrm{Pb}}\right)_{\mathrm{today}} \left(e^{\lambda t} - 1\right) \quad (1)$$

where t represents the time before present and λ represents the decay constant of the parent isotope. In cases where there are only initial (Pb_i) and radiogenic (Pb_r) Pb, this permits the theoretical possibility of calculating three independent ages based on the ^{235}U–^{207}Pb, ^{238}U–^{206}Pb and ^{232}Th–^{208}Pb decay systems. However, several issues limit the general use of Th–U–Pb isochrons: (1) the ^{232}Th has a decay rate that is too slow to provide ages with errors less than 1 Myr, and (2) the ubiquitous presence of modern terrestrial Pb contamination (Pb_c) requires pre-cleaning using dilute acid that typically alters the U/Pb ratio. To circumvent the latter issue, we rely on the dual decay of the U–Pb system that results in unique radiogenic ^{207}Pb/^{206}Pb ratios for different times in the past, by combining the two equations:

$$\left(\frac{^{207}\mathrm{Pb}}{^{204}\mathrm{Pb}}\right)_{\mathrm{today}} = \left(\frac{^{207}\mathrm{Pb}}{^{204}\mathrm{Pb}}\right)_{t_0} + \left(\frac{^{235}\mathrm{U}}{^{204}\mathrm{Pb}}\right)_{\mathrm{today}} \left(e^{\lambda_1 t} - 1\right) \quad (2)$$

$$\left(\frac{^{206}\mathrm{Pb}}{^{204}\mathrm{Pb}}\right)_{\mathrm{today}} = \left(\frac{^{206}\mathrm{Pb}}{^{204}\mathrm{Pb}}\right)_{t_0} + \left(\frac{^{238}\mathrm{U}}{^{204}\mathrm{Pb}}\right)_{\mathrm{today}} \left(e^{\lambda_2 t} - 1\right) \quad (3)$$

Table 1
Half lives and decay constants for isotopes of U and Th as recommended by Villa et al. (2016) after Jaffey et al. (1971) and Le Roux and Glendenin (1963).

Isotope	Half lives	Decay constant
^{232}Th	1.4010×10^{10} years	4.9475×10^{-11} year^{-1}
^{235}U	7.0381×10^{8} years	9.8485×10^{-10} year^{-1}
^{238}U	4.4683×10^{9} years	1.55125×10^{-10} year^{-1}

to derive:

$$\left[\frac{\left(\frac{^{207}\mathrm{Pb}}{^{204}\mathrm{Pb}}\right)_{\mathrm{today}} - \left(\frac{^{207}\mathrm{Pb}}{^{204}\mathrm{Pb}}\right)_{t_0}}{\left(\frac{^{206}\mathrm{Pb}}{^{204}\mathrm{Pb}}\right)_{\mathrm{today}} - \left(\frac{^{206}\mathrm{Pb}}{^{204}\mathrm{Pb}}\right)_{t_0}}\right] = \left(\frac{^{235}\mathrm{U}}{^{238}\mathrm{U}}\right)_{\mathrm{today}} \left(\frac{e^{\lambda_1 t} - 1}{e^{\lambda_2 t} - 1}\right) \quad (4)$$

where the left side of the equation equals the radiogenic (^{207}Pb/^{206}Pb) ratio [(^{207}Pb/^{206}Pb)$_r$] so that Eq. (4) can be reduced to:

$$\left(\frac{^{207}\mathrm{Pb}}{^{206}\mathrm{Pb}}\right)_r = \left(\frac{^{235}\mathrm{U}}{^{238}\mathrm{U}}\right)_{\mathrm{today}} \left(\frac{e^{\lambda_1 t} - 1}{e^{\lambda_2 t} - 1}\right) \quad (5)$$

Eqs. (4) and (5) form the basis for determining ages in (^{206}Pb/^{204}Pb) vs (^{207}Pb/^{204}Pb) space where the slopes of linear arrays correspond to (^{207}Pb/^{206}Pb)$_r$ that define an age (Fig. 1a). Using an "inverse Pb–Pb diagram" that plots ^{204}Pb/^{206}Pb vs ^{207}Pb/^{206}Pb, the intercept of the array corresponds to the Pb isotope composition that lacks ^{204}Pb and must, therefore, equal the radiogenic (^{207}Pb/^{206}Pb) ratio (Fig. 1b). Whether the slope of the array in a standard Pb–Pb plot or the intercept of the inverse Pb–Pb plot should be used to calculate an age depends on the U/Pb ratio of the sample. For highly-radiogenic systems where at least some points fall close to the y-axis of an inverse Pb–Pb diagram, defining the (^{207}Pb/^{206}Pb)$_r$ using the intercept approach of the inverse Pb–Pb diagram will theoretically yield the smallest uncertainty on the age of the two methods. Nearly all the meteoritic samples dated by the Pb–Pb method employ the inverse Pb–Pb method that constrains the intercept rather than the slope and the discussion that follows concentrates on this approach.

Defining an age based on the (^{207}Pb/^{206}Pb)$_r$ ratio (otherwise known as a "Pb–Pb age") requires that any initial Pb incorporated into different phases had a single Pb isotopic composition, that the system remained closed and that the ^{238}U/^{235}U ratio is known for each individual sample (but not the U/Pb ratio). In some rare cases, the sample may not contain any initial Pb such that a pure (^{207}Pb/^{206}Pb)$_r$ component is directly measured. The widespread addition of tetraethyl-Pb to gasoline for over 50 years has contributed to the near ubiquitous contamination of terrestrial Pb in meteorites. As such, this third component of Pb in meteorites must be recognized and, most commonly, removed from the sample for meteoritic Pb isotopic measurements to provide accurate age information.

2.2. ^{238}U/^{235}U composition of the early Solar System

The ^{238}U/^{235}U ratio was assumed to be invariant at 137.88 until Brennecka et al. (2010) showed that significant variations exists in CAIs. However, several recent studies have concluded that the U isotope variability may be limited to the CAI-forming reservoir. Analyses of U isotopic compositions of a eucrite (Juvinas), an unclassified basaltic meteorite (NWA 2976), an enstatite chondrite (Sahara 97159), a CI chondrite (Ivuna), a CB chondrite (Gujba), three chondrules from CV3 Allende and an L3 ordinary chondrite (NWA 5697) returned overlapping compositions with an average value of 137.786 ± 0.011 (Connelly et al., 2012). This result is in agreement with the analyses of six

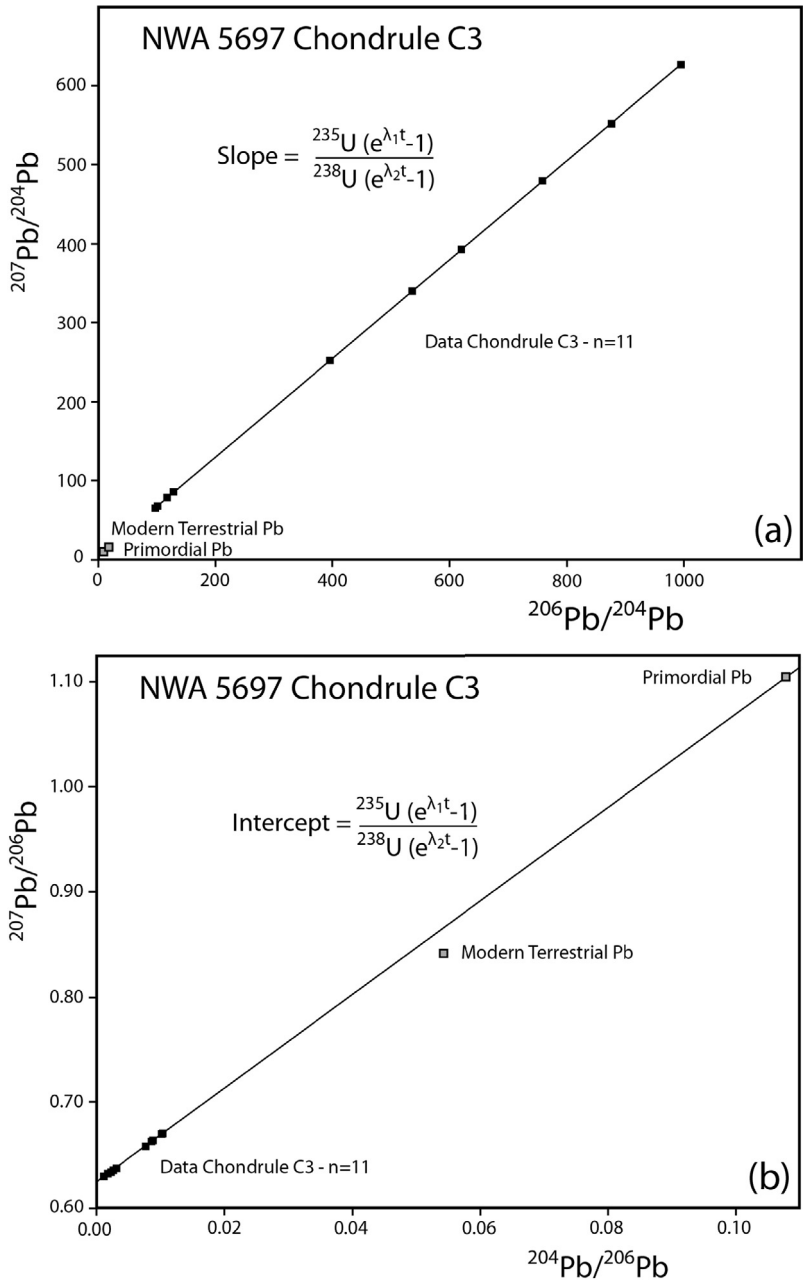

Fig. 1. (a) Standard Pb–Pb diagram where the age is determined using the $(^{207}Pb/^{206}Pb)_r$ isotopic ratio corresponding to the slope of the isochron. (b) Inverse Pb–Pb diagram with the same data shown in (a) but where the age is determined by the $(^{207}Pb/^{206}Pb)_r$ isotopic composition corresponding to the *y*-intercept of the isochron. Data for these plots are for chondrule C3 from NWA 5697 in Connelly et al. (2012). Decay constants λ_1 and λ_2 are for ^{235}U and ^{238}U, respectively, and t represents the time past since closure of the U–Pb system.

angrites by Brennecka and Wadhwa (2012) who reported an average value of 137.780 ± 0.021. Finally, Brennecka et al. (2015) reported on the U isotopic compositions of pooled chondrules for Allende as well as bulk Allende and matrix from Allende that were overlapping with an average value of 137.786 ± 0.004. These results support two important conclusions about the U isotopic composition of the early Solar System. First, the analyses of these diverse materials including CAI-free chondrites, chondrules and several differentiated bodies strongly supports homogeneity of U in the Solar System outside of the CAI-forming region with a present-day value of 137.786 ± 0.011. Second, fractionation of U during high-temperature thermal and magmatic processing has not been documented in these studies within the analytical uncertainties.

There are two studies that report U isotopic composition for early Solar System materials outside of this limit, namely Goldmann et al. (2015) and Kaltenbach (2012). Goldmann et al. (2015) analyzed a range of chondrites,

eucrites and angrites as well as six achondrites, three of which are unique meteorites. The eucrites, angrites and achondrites overlap the value of 137.786 ± 0.011. However, when scrutinizing the chondrite data set of Goldmann et al. (2015), serious issues become apparent. The reported $^{238}U/^{235}U$ variability, mostly expressed in ordinary chondrites of high metamorphic grade, is positively correlated with the U content. This behavior is expected if the $^{238}U/^{235}U$ variability reflects stable U isotope fractionation associated with the mobilization of phosphates during metamorphism. We note that the size of the samples characterized by $^{238}U/^{235}U$ variability were typically small (500–600 mg), which makes these measurements highly susceptible to the heterogeneous distribution of phosphates. Indeed, much larger samples (>5 g) of high metamorphic grade ordinary chondrites measured in the same study did not show $^{238}U/^{235}U$ variability. Thus, we conclude that the bulk of the $^{238}U/^{235}U$ variability reported by Goldmann et al. (2015) is secondary and due to unrepresentative sampling of the chondrites.

When examining the data of the second study by Kaltenbach (2012) in a critical fashion, CAI-free type 3 chondrites with acceptable errors (i.e. <1.5 epsillon units), the analyses of three EH3 chondrites, eucrites and seven angrites return a U isotopic composition that overlaps that of Connelly et al. (2012). One eucrite represents an obvious outlier in the data, namely the eucrite Agoult with a $^{238}U/^{235}U$ value of 137.708 ± 0.016. The rest of this data set comprises CAI-bearing CV chondrites and hydrated chondrites that should not be used to define the U isotopic composition of the protoplanetary disk. A single analysis of pooled presumed chondrules from a CAI-bearing chondrite yield a U isotopic composition of 137.724 ± 0.031. This value is significantly lower than that measured for three single Allende chondrules by Connelly et al. (2012) and aliquots of pooled chondrules by Brennecka et al. (2015) all with values overlapping 137.786 ± 0.11. However, it is difficult to evaluate the significance of the Kaltenbach (2012) chondrule result as the incorporation of minute amounts of CAIs in their pooled chondrules aliquot could readily lead to a sub-solar $^{238}U/^{235}U$ ratio.

In summary, there appears to be a convergence in these five studies towards the value of 137.786 ± 0.011 defined by Connelly et al. (2012) for the present-day bulk Solar System U isotope composition. We recognize that some metamorphosed chondrites yield $^{238}U/^{235}U$ values outside of 137.786 ± 0.013 (Kaltenbach, 2012; Goldmann et al., 2015), but we attribute this to fractionation induced by secondary processing or, possibly, analytical artifacts associated with measuring small amounts of U. These studies support the use of a solar U isotope composition of 137.786 ± 0.011 to calculate Pb–Pb ages of meteoritic material but we emphasize that the U isotopic composition should be verified whenever possible.

3. SOURCES OF PB IN METEORITES AND THEIR COMPONENTS

The most common scenario for meteoritic materials will be a two-component system of initial and radiogenic Pb mixed with a third component of terrestrial Pb contamination (which may represent multiple sources with slightly different isotopic compositions). The relative proportion of Pb_r and Pb_i will depend on the U/Pb ratio of the sample, most conveniently expressed as the $^{238}U/^{204}Pb$ ratio or μ value. In samples containing Pb_i, calculating a Pb–Pb age requires the removal of Pb_c to construct an array based on mixtures of only Pb_r and Pb_i that accurately points to the correct isotopic composition of Pb_r on the y-axis (Connelly and Bizzarro, 2009). With Pb_c typically being more labile than Pb bound in minerals as Pb_i, the removal of this component may be accomplished by pre-cleaning the sample with a variety of reagents including water, acetone, ethanol and dilute acids (HBr and HNO_3) on a hotplate and with ultrasonication before dissolution of mineral phases with Pb_r and Pb_i with more concentrated acids (Connelly and Bizzarro, 2009). Cleaning is thought to be aided by at least coarsely crushing the sample prior to the cleaning procedure but removal of all the Pb_c is not assured despite extensive efforts. In these cases, points will be pulled off the isochrons towards the isotopic composition of Pb_c. For ancient meteorites, this causes points to plot below the true $Pb_r + Pb_i$ array (Fig. 2). If this problem persists for most or all of the analyses from a single sample, the data will fail to define a statistically acceptable line such that no meaningful age information can be extracted.

In some rare cases, samples will not contain any measurable Pb_i so that they may contain a two-component mixture of Pb_c and Pb_r. Pre-cleaning these samples will result in more radiogenic residues but the washes that preferentially contain Pb_c and residues that preferentially contain Pb_r will define a single array with a y-intercept that accurately reflects the Pb_r isotopic composition (Fig. 3). This condition is identified by checking that the projection of the line to less radiogenic isotopic compositions passes through a value of Pb_c consistent with reasonable estimates of average modern terrestrial Pb that may be contaminating that meteorite (e.g. Bollard et al., 2015). The contaminant Pb may have been acquired from one or more sources but the most robust contaminant Pb is likely acquired over longer time periods in the field before the meteorite was discovered. One might expect that desert meteorites would contain negligible Pb_c due to the dry conditions, but this has not proven to be the general case (eg. SAH99555; Connelly et al., 2008; Amelin, 2008a; Gujba; Bollard et al., 2015) and this component of Pb can persist through aggressive cleaning and even into the dissolution steps. It is important to reiterate that a two-component Pb isotopic array of pure Pb_r mixed with Pb_c will yield an isochron pointing to an appropriate $(^{207}Pb/^{206}Pb)_r$ ratio that corresponds to the correct age for that meteorite.

4. GENERATING A PB–PB ISOCHRON

As stated above, the main requirement of the Pb–Pb method is to define a statistically acceptable array that necessitates reducing the system to not more than two components, either $Pb_r + Pb_i$ or $Pb_r + Pb_c$. Since most samples will contain some Pb_i, the challenge is more typically to remove Pb_c first and then define an isochron representing

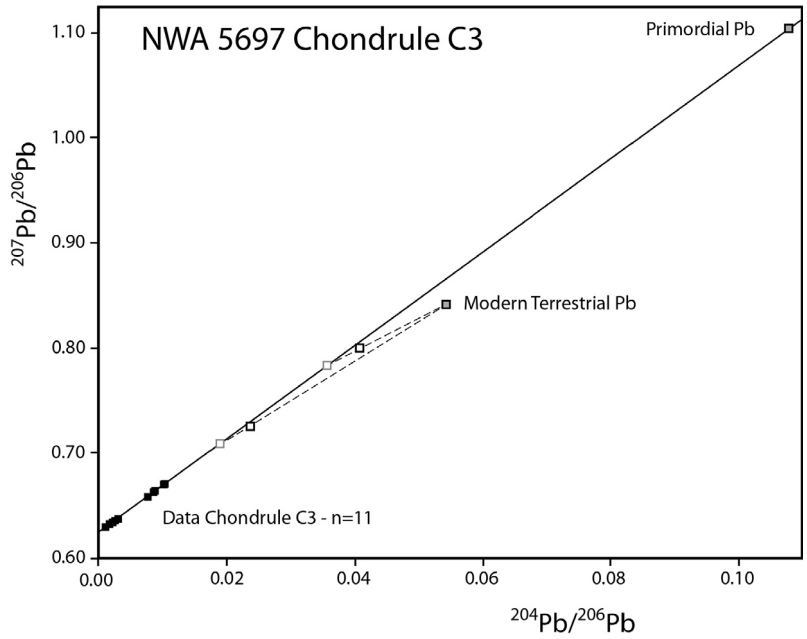

Fig. 2. Pb isotopic data for chondrules C3 from NWA 5697 (Connelly et al., 2012) plus two synthetic points showing the effect of these fractions containing a component of modern terrestrial Pb. Two points that should have plotted on the isochron (light open squares) are translated towards modern terrestrial Pb resulting in analyses that plot below the isochron (heavy open squares).

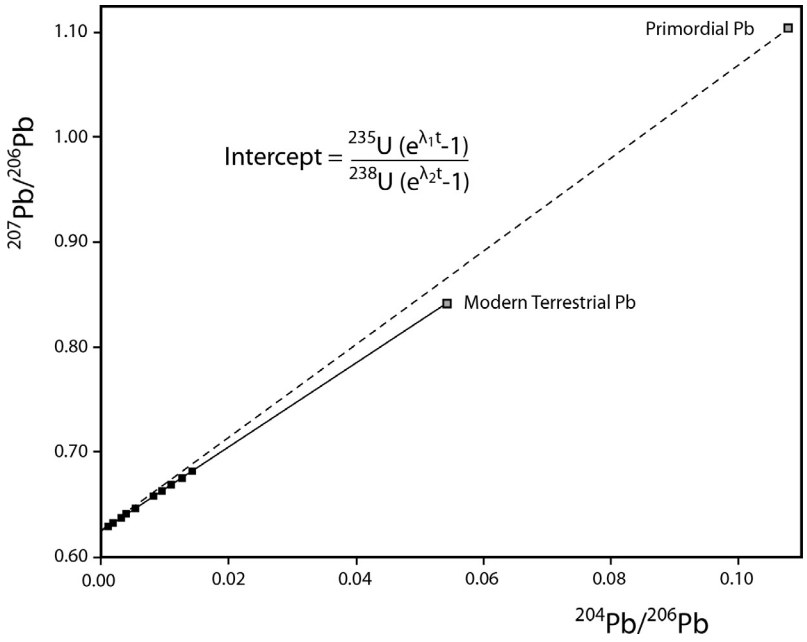

Fig. 3. Meaningful y-intercepts corresponding to the correct radiogenic $^{207}Pb/^{206}Pb$ ratio for a sample can be calculated from two component mixtures of either $Pb_r + Pb_i$ or $Pb_r + Pb_c$. This example shows synthetic data representing a mixture of $Pb_r + Pb_c$ with the dashed line showing the corresponding isochron for an object of the same age but with a $Pb_r + Pb_i$ mixture. The solid line of this example is technically not an isochron because the distribution of points reflects mixing rather than ingrowth of different amounts of radiogenic Pb.

$Pb_r + Pb_i$. There are two main approaches. The first method involves physically separating, cleaning and analyzing different minerals with an appropriate range of μ-values to define a Pb_r–Pb_i array. This allows individual fractions to be extensively cleaned while visually monitoring whether the sample is being dissolved by the acids used for pre-cleaning, permitting the use of more concentrated and aggressive acids in the cleaning steps without concern that an important component of the sample is being removed. In this method, the number of data points defining an isochron is limited by the number of mineral fractions prepared. This method is only amenable to samples with

sufficiently large grain sizes that allows for their physical separation and purification.

The second method is to process a coarsely-crushed whole rock aliquot of appropriate size by first cleaning with water, acetone and ethanol and very dilute acids before a progressive dissolution routine using increasingly aggressive acids until a final residue is fully dissolved with a full strength $HF–HNO_3$ mixture. Given that the different acids and strengths preferentially dissolve different phases or combination of phases throughout the dissolution sequence, the Pb is parsed into mixtures of Pb_r and Pb_i that will define an isochron. As it is not known in real time when processing mineral separates whether all the Pb_c is successfully removed, this method has the advantage of additional opportunities to remove any Pb_c left after pre-cleaning in the early dissolution steps. In this case, even samples with more persistent Pb_c can yield a $Pb_r + Pb_i$ isochron using a subset of the advanced dissolution steps. There are no statistical guidelines about how many points are required to define a meaningful isochrons but confidence is diminished in an age based on a low percentage of total dissolution steps. One should also pay attention to the total amount of Pb in each fraction, given that fractions with a low sample/blank ratio are less reliable than those with a high sample/blank ratio. An isochron defined by a subset of dissolution steps containing the largest amounts of Pb should be considered more reliable than one with points containing smaller amounts of Pb. Questions about this method have arisen regarding the potential for the progressive stepwise acid dissolution procedure fractionating Pb isotopes and the significance of those cases where some advanced dissolution steps, including the residual fraction, do not fall on the main array used to define an isochron. The following sections address these issues.

4.1. Non-mass dependent fractionation of Pb isotopes during processing

The near ubiquitous requirement to remove Pb_c from meteoritic material using some types and strengths of acids raises the possibility of fractionating Pb_r isotopes (Amelin et al., 2009, 2016). This concern is rooted in the fact that the radiogenic ^{206}Pb is produced from ^{238}U with one more alpha decay than the production of ^{207}Pb from ^{235}U, leaving $^{206}Pb_r$ in a slightly more damaged site than $^{207}Pb_r$. Processing pure mineral separates may be less susceptible to this issue if more dilute acids are used in the pre-cleaning than are required to attack the silicate structures hosting the Pb. A greater concern lies in progressive dissolution methods where there is a continuum of dissolution of different phases throughout the routine starting with carbonates and phosphates and ending with the more robust silicates and oxides. It is predicted that fractionation would be accomplished by first preferentially removing $^{206}Pb_r$ from the more damaged sites early in the dissolution series, followed by fractions enriched in $^{207}Pb_r$ in the later stages (Amelin et al., 2009). This would be expressed as points early in the dissolution series plotting below the isochrons and points later in the series above the isochron. There is a hint in several data sets that this may occur, with the problem expected to be most obvious where concentrated acids with a strong affinity of Pb (e.g. 9 M HBr) is applied early in the dissolution process (Amelin et al., 2010). While it is possible to establish tailored tests of this effect on either meteoritic or terrestrial material, the results will ultimately be difficult to apply to future studies. In the case of a test determining that Pb_r fractionation is possible for certain minerals under certain combinations of acids, temperatures and duration, there is no way to know whether this will occur in other samples. Conversely, if a set of tests fails to document Pb_r fractionation, there are no assurances that it cannot happen in other samples.

Despite this caveat, a test of whether this method can systematically return meaningful isochrons has effectively been conducted in a study dating four individual chondrules from the Cba meteorite Gujba. These chondrules are thought to have formed coevally from an impact plume after the high-energy collision of two planetesimals. Bollard et al. (2015) reported four chondrules with overlapping ages for the stepwise dissolution Pb–Pb method. The arrays for each chondrule were defined by at least half of the fractions analyzed to define a weighted means average age of 4562.49 ± 0.21 Ma (MSWD = 0.41). Of the 47 dissolution steps for the four chondrules, 37 fractions were used to define the four individual isochrons. Additionally, 31 of the 47 dissolution steps define a composite isochron corresponding to an age of 4562.47 ± 0.22 Ma (MSWD = 1.02), an age in perfect agreement with the weighted means average age of the four individual isochrons, confirming their co-genetic formation.

Despite this successful test of the method for this meteorite, the only viable assessment of others sample lies in the arrangement of the data points in Pb–Pb space. Colinearity of all fractions guarantees that Pb_r fractionation has not occurred and provides the highest confidence level in the age based on such an array. Cases where points falling off the isochron lie only on one side towards Pb_c lack the necessary complimentary high $^{207}Pb/^{206}Pb$ component that would be required by Pb_r fractionation and, therefore, must reflect varying degrees of contamination of Pb_c. In this case, the isochron defined by an upper bounding surface of the data points should be considered robust. Confidence in the age will be lowest for cases with multiple data points both above and below an isochron that is defined by relatively few of the dissolution steps that contain a low percentage of the total Pb. Using this logic, each data set for a single sample and age should be assessed for the likelihood that Pb_r fractionation might have occurred and assign a qualitative confidence in the age accordingly.

4.2. Characterizing the most radiogenic phase(s) in chondrules

For the method exploiting purified mineral fractions, it is expected that the residual component left after cleaning steps by different solvents and acids should provide the purest measurements of different mixtures of Pb_r and Pb_i. A pure mineral separate with a homogeneous distribution of U and Pb_i should reproducibly yield the same Pb isotopic composition if all Pb_c is removed. In contrast, the stepwise

dissolution of a coarsely-crushed whole rock will yield a range of Pb isotopic compositions as the different acids and acid strengths attack different phases at different rates that are not reproducible from one sample to the next. Moreover, the most radiogenic fraction need not come from the final residue given that the most resistant phase to the HF–HNO_3 acid mixtures may not have the highest μ value. In fact, the first steps that expose the sample to HF consistently liberates the most radiogenic Pb in almost all meteoritic materials dated by this method (Connelly and Bizzarro, 2009). To evaluate the significance of this observation, the different major phases of several chondrules were analyzed to determine which phase contains the most radiogenic Pb, and, therefore, possesses the highest μ value. Using the secondary ion mass spectrometry (SIMS) at the Swedish National History Museum in Stockholm, Bollard (2016) measured the Pb isotopic composition of coarse pyroxene, olivine and pyrite as well as the fine-grained mesostasis that comprises plagioclase and micrometer dendrites of high-Ca pyroxene in two chondrules (Fig. 4a). In both samples, the radiogenic Pb resides in the mesostasis (Fig. 4b) whereas the amount of Pb in both coarse-grained pyroxene and olivine was more than an order of magnitude lower in Pb concentration and less radiogenic. The ion beam size was not small enough to measure the plagioclase and micrometer dendrites of pyroxene separately, but available U–Pb coefficients for these two minerals predict that the U preferentially resides in the pyroxene. The isotopic composition of pyrite overlapped that of primordial Pb indicating it has a μ-value of ~0 (Fig. 4b). For at least these two chondrules, the Pb for most of the stepwise dissolution steps is predominantly a binary mixture of Pb

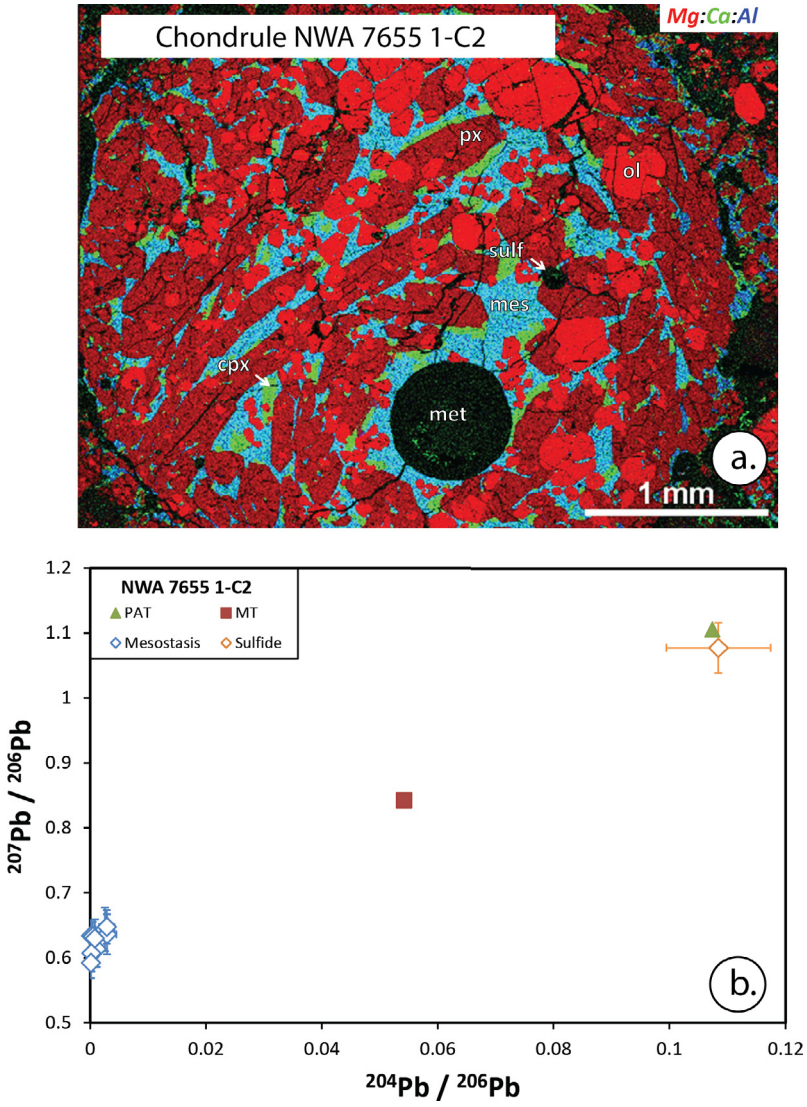

Fig. 4. (a) Mg–Ca–Al elemental map of chondrule NWA 7655 1-C2 where px = pyrozene, ol = olivine, cpx = clinopyroxene, mes = mesostasis, met = metal, sulf = sulfide. (b) An inverse Pb–Pb diagram of secondary ion microprobe mass spectrometer analyses of highly-radiogenic Pb in mesostasis and unradiogenic Pb in sulfide in a chondrule from NWA 7655 where PAT = primordial Pb and MT = modern terrestrial Pb. Both image and plot from Bollard (2016).

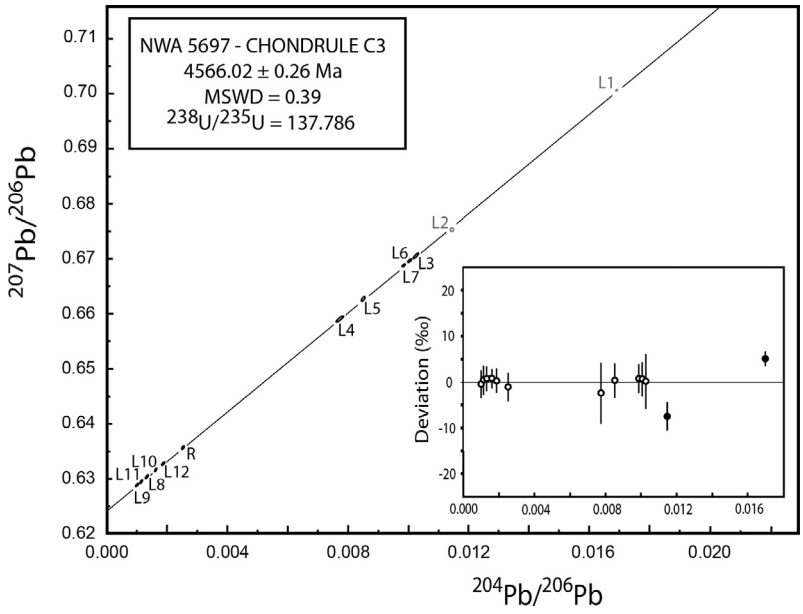

Fig. 5. Inverse Pb–Pb diagram for chondrule C3 from CV meteorite NWA 5697 reproduced from Connelly et al. (2012). Inset shows deviations of each analyses from the isochron in parts per thousand, with errors bars on each point corresponding to the total $^{207}Pb/^{206}Pb$ error of each analyses. Open symbols correspond to those fractions used in defining the isochron whereas black symbols were excluded in the regression. L = partial dissolution step; R = residue.

from pyrite and the mesostasis with a third component of labile Pb_c effectively removed by pre-cleaning and the early dissolution steps (Bollard, 2016). Presuming a higher reactivity of the fine-grained mesostasis of plagioclase and micometer-scale pyroxene and inert behavior of pyrite in HF, the liberation of the most radiogenic Pb by the first use of HF (without HNO_3) is viewed as consistent with this phase containing the highest μ-value.

5. EVALUATING PB–PB DATA FROM THE STEPWISE DISSOLUTION METHOD

For the sake of illustrating how to assess the robustness of an individual Pb–Pb age by the stepwise dissolution method, we present two successful examples from Connelly et al. (2012) and a third unpublished example that failed. All three samples were processed by lightly crushing a fragment of an inclusion that had surrounding matrix removed by a diamond-coated wire saw and/or a hand-held Dremmel™ tool. They were pre-cleaned by water–ethanol–acetone cycles followed by dilute (<0.1 M) HBr and HNO_3.

Chondrule C3 from the L3.10 CV chondrite NWA 5697 yielded an age of 4566.02 ± 0.26 Ma based on 11 of 13 dissolution steps, with only the first two steps falling off the isochron (Connelly et al., 2012). The 11 fractions defining the statistically acceptable array (Fig. 5) as defined by Isoplot (Ludwig, 2003) comprise 2.43 ng of Pb relative to the two, least radiogenic points falling off the array that contain 0.56 ng. The most radiogenic fraction contains 0.47 ng of Pb, making it relatively unsusceptible to the relatively large uncertainty on the 0.5 pg of Pb blank. Finally, the isochron projects back to a Pb isotopic composition that is compatible with the primordial Pb isotopic composition of the Solar System. While this is not a pre-requisite condition of obtaining a robust Pb–Pb age, it provides additional confidence that the isochron is not rotated by the inclusion of an unidentified Pb component. The three most radiogenic fractions overlap and contain 0.18–0.67 ng of Pb, making them relatively unsusceptible to the blank correction. Collectively, this data sets represents a near perfect scenario with only first two dissolution steps falling off the isochron.

The second example of a chondrule comes from the CR2 chondrite NWA 801. In this case, 18 washes and dissolution steps were analyzed following the methods of Connelly et al. (2012) but the data failed to define a coherent array that could be used to determine a line and intercept (Table 2 and Fig. 6). The data plot above and below a 4565.5 Ma reference isochron, indicating that Pb was redistributed in an unidentified secondary alteration event and that modern terrestrial Pb may have been a significant component of the Pb in this chondrule. This sample stands in stark contrast to chondrule C3 from NWA 5697 and clearly demonstrates the difference between a datable sample that fulfills all necessary conditions to determine a reliable isochron age and one that cannot be dated because it has experienced post-crystallization partial re-equilibration and/or contains extensive contamination by modern terrestrial Pb.

The third example represents a fine-grained CAI (22E) that was recovered from the CV chondrite Efremovka. The texture and mineralogy of this CAI is consistent with its formation by condensation of a gas phase (Connelly et al., 2012). Eight of 12 fractions from the main dissolution series define a well-correlated isochron (Fig. 7) with another four of eight pre-washes also lying on this line, for a total of 12 well-constrained fractions defining the isochron. An additional 4 fractions (W1-4, W10, W11 and L4: Fig. 7 inset) with larger errors also overlap the isochron (Fig. 7,

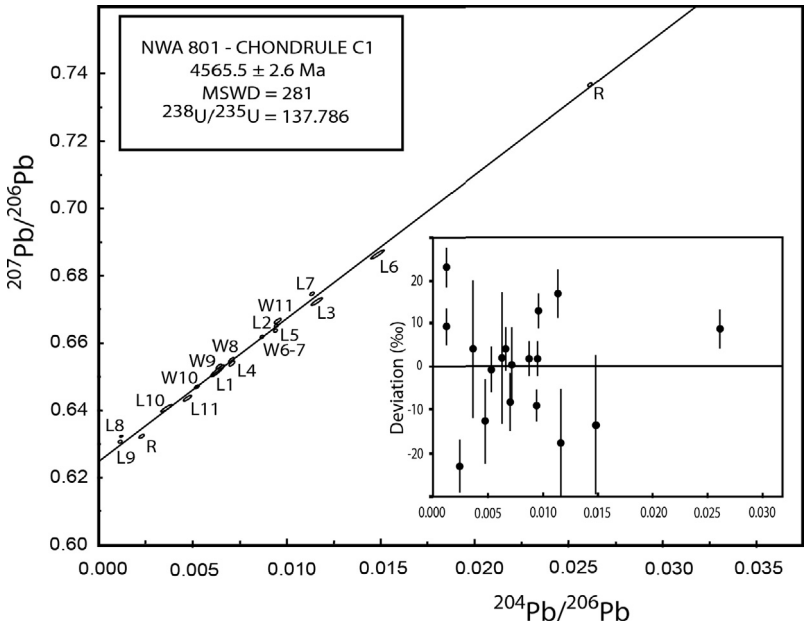

Fig. 6. Inverse Pb–Pb diagram for chondrule C1 from CR2 meteorite NWA 801 with a reference isochron line corresponding to an age of 4565.5 ± 2.6 Ma. Inset shows deviations of each analyses from the isochron in parts per thousand, with errors bars on each point corresponding to the total $^{207}Pb/^{206}Pb$ error of each analyses. L = partial dissolution step, W = wash step, R = residue.

insert a) but do not affect the age and error derived from the 12 better-constrained fractions. There is a total of 3.25 ng of Pb (with fractions ranging from 0.27 to 0.79 ng of Pb) in this sample such that the blank subtraction of 1 pg with its uncertainty contributes an insignificant amount of error to the final calculated ratios. Of the 12 fractions of the main dissolution series that do not fall on the isochron, one (*R*) plots below the line consistent with a minor component of terrestrial common Pb remaining in the samples having been removed by these acid steps. The single fraction (L5) that plots slightly above the isochron by 17 ± 3 ε units (parts per 10^4) represents an early HCl dissolution step. If this one fraction reflects some degree of induced Pb isotopic fractionation in an enhanced $^{207}Pb/^{206}Pb$ ratio, it is minor in comparison to the number of points and the amount of Pb in the fractions defining the isochron and can be balanced by the analyses that lie below the isochron. Finally, the isochron projects back through the isotopic composition of primordial Pb, indicating a mixture of Pb_r and a component of non-radiogenic Pb that may have originated in the matrix (see discussion below). Whereas only 2 of 12 main dissolution data points fall statistically off the isochron, the remaining fractions contain sufficient Pb to make them insensitive to the blank correction. Evaluating all this information collectively, we conclude that the isochron age is robust within the uncertainties stated.

The assessment of these three examples demonstrate the most critical attributes of any data set generated by the stepwise dissolution method to be examined, which can be summarized as follows:

- First and foremost, the data must convincingly define a statistically-acceptable linear array.
- The number of analyses defining an isochron should exceed those rejected with those samples with the highest acceptance rate providing the greatest confidence.
- The amount of Pb analyzed in at least a subset of fractions should be large enough to be relatively insensitive to the blank correction.
- The data array should be checked for evidence of mass independent fractionation that could compromise the calculated $(^{207}Pb/^{206}Pb)_r$.
- If there is Pb_i present in the sample, the back projection of the isochron to non-radiogenic Pb should point to a composition consistent with the earlier history of the sample or its precursor material.
- For any sample modeled as being free of Pb_i, the back projection of the isochron to non-radiogenic Pb should point to an isotopic composition that is consistent with modern terrestrial Pb.

Any compilation of ages must recognize that various levels of confidence exists for different data sets and that added weight should be given to those samples/ages that fulfill more criteria.

6. MASS SPECTROMETRY OF PB ISOTOPES

Two types of mass spectrometers are mainly employed to measure U and Pb isotopic compositions in meteoritic materials with sufficient precision to determine useful Pb–Pb ages. Both types separate the isotope masses by a magnetic sector and are equipped with multiple faraday detectors for larger beams and one or more ion counting channels for smaller beams. The main difference between these designs lies in the method used to ionize the atoms.

Table 2
Pb isotope data for NWA801 chondrule.

	Acid	Pb (pg)	$^{206}Pb/^{204}Pb_{raw}$	$^{204}Pb/^{206}Pb_{corr}$	2SE (%)	$^{207}Pb/^{206}Pb_{corr}$	2SE (%)	Rho	$^{208}Pb/^{206}Pb_{corr}$
W6-7	Dilute HBr	64.9	111.7	0.008696	0.69	0.661819	0.041	0.848	1.15534
W8	Dilute HBr	28.9	130.5	0.007114	1.93	0.654969	0.084	0.967	1.13130
W9	Dilute HBr	50.9	145.1	0.006572	1.18	0.653016	0.051	0.909	1.11115
W10	Dilute HBr	49.5	177.9	0.005290	1.54	0.647117	0.054	0.919	1.08880
W11	Dilute HBr	22.7	97.6	0.009568	1.76	0.666637	0.100	0.975	1.16596
L1	1 M HBr	16.0	137.8	0.006289	4.07	0.651589	0.152	0.989	1.10908
L2	2 M HCl	60.2	102.2	0.009512	0.66	0.665280	0.042	0.855	1.11658
L3	3 M HNO_3	17.2	80.0	0.011624	1.86	0.672284	0.127	0.982	1.20143
L4	4 M HNO_3	36.9	132.6	0.007116	1.48	0.654092	0.066	0.946	1.08397
L5	2 M HCl	73.6	103.5	0.009434	0.55	0.663873	0.037	0.804	1.11375
L6	6 M HCl	12.5	62.6	0.014846	1.89	0.686385	0.160	0.986	1.23553
L7	6 M HCl	40.5	85.1	0.011360	0.78	0.674624	0.056	0.898	1.08774
L8	1 M HF	218.9	761.2	0.001238	1.51	0.632284	0.024	0.490	0.94913
L9	1 M HF	74.1	718.7	0.001177	4.89	0.630653	0.040	0.860	0.96879
L10	7 M HF	15.8	218.8	0.003613	7.41	0.640498	0.157	0.985	0.98979
L11	7 M HF	25.9	187.1	0.004747	3.28	0.643625	0.096	0.975	1.02271
L12	28 M HF – 14 M HNO_3	43.2	371.1	0.002332	4.13	0.632304	0.063	0.943	0.97417
R	28 M HF – 14 M HNO_3	35.4	37.6	0.026163	0.31	0.736654	0.045	0.796	1.48360

Sample subjected to a precleaning routine of 5 cycles of ethanol, acetone and water on the hotplate and ultrasonic followed by 5 steps of 0.02 M HBr on a hotplate (15 min) and ultrasonic bath (5 min).
The $^{206}Pb/^{204}Pb_{raw}$ reflects the measured $^{206}Pb/^{204}Pb$ ratio. All other ratios are corrected for mass fractionation (using a $^{205}Pb/^{202}Pb$ tracer), blank contribution and spike addition with these uncertainties on these corrections propagated to the quoted uncertainties.
The Rho value is the error correlation between $^{204}Pb/^{206}Pb$ and $^{207}Pb/^{206}Pb$ ratios.

For Thermal Ionization Mass Spectrometers (TIMS), a sample of purified Pb is loaded onto Re filaments as a solid salt that will be heated to temperatures between 1200 and 1600 °C to gradually evaporate and ionize the Pb atoms over several hours. For Multi-Collector Inductively Coupled Plasma Mass Spectrometers (MC-ICP-MS), a purified Pb sample in a dilute HNO_3 solution is aspirated into the +5000 °C plasma that ionizes nearly 100% of the atoms. Whereas the MC-ICP-MS has a much higher ionization efficiency than TIMS, the ion yield of Pb to the detectors are similar, typically between 0.5 and 5.0% depending on the configuration of the instrument. A full discussion of the benefits and drawbacks of the two methods is beyond the scope of this review, but the following lists the main issues to consider when selecting the most appropriate instrument for a given application in Pb–Pb geochronology.

6.1. Sample size for Pb analyses

The stable beam intensity and low (to zero) backgrounds of TIMS lends itself to running amounts of Pb as low as ~1 pg while obtaining useful precision and reproducibility (e.g. Borg et al., 2011). This reflects the fact that a single ion-counting channel (with backgrounds less than a count per minute) can be used to sequentially measure the respective Pb masses, compensating for the slowly-evolving but relatively-stable ion beams. The plasma source of an MC-ICP-MS generates a less stable ion beam intensity, typically precluding the use of a single ion counter to sequentially measure different Pb masses in a single ion counting system on these instruments. Commercially available multiple ion-counting channels may eventually avoid this problem, but the relative inter-channel calibrations of multiple ion-counting systems have not yet been demonstrated to be stable enough to make this solution practical at present (Amelin and Huyskens, 2013). As such, TIMS is the preferred instrument for small samples or aliquots of samples containing less than 20 pg of total Pb. Other factors guide the decision of which instrument is more practical for larger samples.

6.2. Assessing instrumental mass fractionation

Both TIMS and MC-ICP-MS instruments induce mass dependent fractionation of Pb isotopes. The main source of fractionation in TIMS analyses lies in the preferential evaporation of the lighter Pb isotopes over the heavy isotopes typically in the range of 0.1–0.2%/atomic mass unit (amu). For MC-ICP-MS analyses, mass fractionation mainly reflects the preferential transmission in the range of 1%/amu of the heavier isotopes of Pb. For TIMS, correction for mass dependent fractionation is typically accomplished by adding a mixed ^{202}Pb–^{205}Pb tracer of known isotopic composition to samples to be analyzed. An accurate correction depends on an appropriate mass fractionation law so that the amount of fractionation measured over the 3 mass units between ^{202}Pb and ^{205}Pb can be applied to the unknown Pb isotope ratios that typically represent one or two amu differences. The limited amount of artificially-produced ^{202}Pb and ^{205}Pb that is currently available makes this method of mass fractionation correction mostly unavailable to the MC-ICP-MS approach because of the larger amounts of Pb required by this method. Correction for instrumental mass fractionation on the MC-ICP-MS is accomplished by sample-standard bracketing with or without the addition of thallium to the sample after

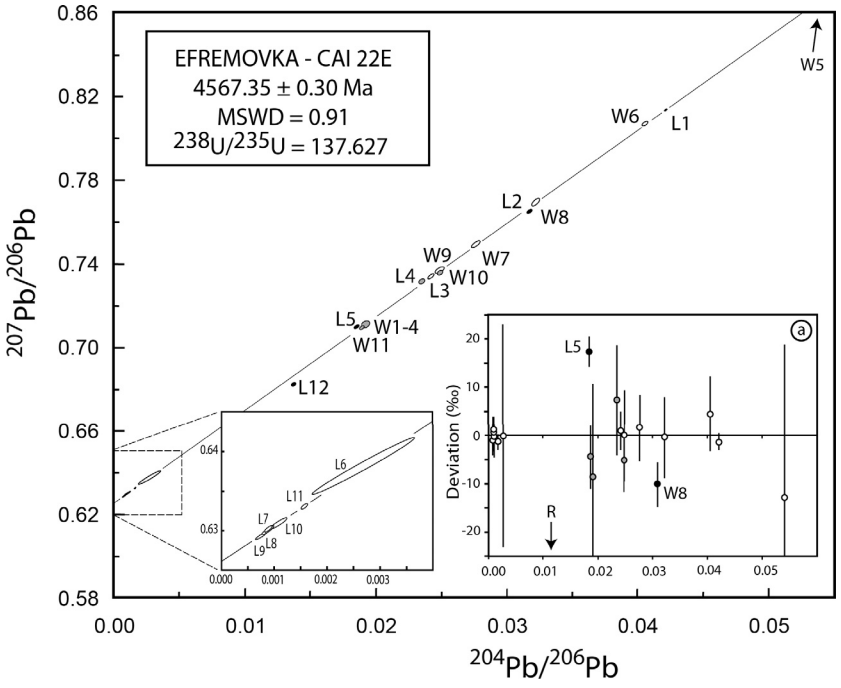

Fig. 7. Inverse Pb–Pb diagram for CAI 22E from CV meteorite Efremovka reproduced from Connelly et al. (2012). Inset (a) shows deviations of each analyses from the isochron in parts per thousand, with errors bars on each point corresponding to the total $^{207}Pb/^{206}Pb$ error of each analyses. Open symbols correspond to those fractions used to define the isochron, gray symbols overlap the isochron and black symbols do not overlap the isochrons (see text for discussion). W = wash step, L = partial dissolution step, R = residue.

Pb purification. Sample-standard bracketing requires that the samples and standards are comparably clean of matrix elements, else the degree of fractionation may differ between them. The use of ^{203}Tl–^{205}Tl to correct for mass fractionation permits an internal normalization (Kamenov et al., 2004) but requires that Tl and Pb behave in a predictable manner between standards and samples. For information for and against the applicability of using Tl as an internal normalization guide see White et al. (2000) vs Baker et al. (2004). The use of double spikes of naturally occurring Pb isotopes such as a ^{207}Pb–^{204}Pb (e.g. Thirlwall, 2000; Baker et al., 2004) is typically precluded by the insufficient amount of Pb in single samples to make the necessary analyses of spiked and unspiked aliquots.

6.3. Measuring the minor isotope ^{204}Pb relative to major isotope ^{206}Pb

Determining the $^{204}Pb/^{206}Pb$ ratio of a sample may require measurement of an extreme ratio for highly-radiogenic materials. It is most common for MC-ICP-MS analyses to measure ^{204}Pb in an axial secondary electron multiplier with all other isotopes measured simultaneously in faraday collectors coupled to amplifiers with appropriate-sized resistors. This approach results in a cross-platform measurement between at least one secondary electron multiplier and one faraday cup for the critical $^{204}Pb/^{206}Pb$ ratio. An accurate ratio determination requires careful calibration of the secondary electron multiplier – ion counting system relative to the appropriate faraday detector, a parameter that fluctuates/drifts continuously. There is no clear routine outlined in recent MC-ICP-MS papers explaining how the secondary electron multiplier relative to faraday detectors is cross-calibrated and monitored throughout an analytical session (eg. Bouvier and Wadhwa, 2010; Bouvier et al., 2011). Further, there is also typically no assessment for MC-ICP-MS studies of the non-linearity of SEM response over the working range from low count rates of 1000 cps to the upper register of more than 1×10^6 cps or an evaluation of the effective dead-time of the SEM-IC amplifier. It is important to note that a 10% offset in the corrected ^{204}Pb intensity for a sample with a $^{204}Pb/^{206}Pb$ ratio of 0.001, such as reported for standards by Bouvier and Wadhwa (2010), corresponds to an offset of ~1 Myr in the model $^{207}Pb/^{206}Pb$ age with Pb_i defined by primordial Pb. As such, the faraday – SEM-IC calibration method as well as the dead-time and linearity of the SEM-IC system on MC-ICP-MS must be carefully documented and reported.

The more stable ion beam of a TIMS analysis permits the use of a peak-jumping routine where all Pb isotopes are measured on a single ion counting system. This allows for using different combinations of detectors such that no critical ratio uses a cross-platform measurement (e.g. Connelly and Bizzarro, 2016). For small samples, all masses are sequentially measured on a single axial ion counting system. This provides direct comparisons of beam intensities on a single detector that avoids cross-detector calibrations but that still requires that any non-linearity effects and mass dependent discrimination must be monitored and corrected. For large samples, ^{202}Pb, ^{204}Pb and ^{205}Pb are analyzed sequentially on the axial SEM-IC detector

(with corrections for non-linearity and mass dependent discrimination effects of the ion counting system) with masses ^{206}Pb, ^{207}Pb and ^{208}Pb simultaneously analyzed on faraday detectors during the step with ^{204}Pb in the axial detector. This provides all critical ratios determined by a single detector type except for the ^{204}Pb/^{206}Pb ratio. This ratio can be measured using a second method with the filament temperature reduced to allow ^{207}Pb, ^{206}Pb and ^{204}Pb to be measured sequentially on the SEM-IC (a maximum signal of $0.6–1.2 \times 10^6$ cps is typically adapted for ion counting systems). In this routine, internal fractionation correction for the ^{204}Pb/^{206}Pb ratio is determined by the ^{207}Pb/^{206}Pb ratio, which is known from the static faraday measurement that uses the dynamically determined ^{205}Pb/^{202}Pb ratio to internally normalize.

6.4. Enhanced mass fractionation of odd mass isotopes

Several TIMS studies have demonstrated the potential for anomalous fractionation of ^{207}Pb relative to the other even-mass isotopes of Pb that does not occur in MC-ICP-MS analyses (Thirlwall, 2000; Doucelance and Manhès, 2001; Amelin et al., 2005; Villa et al., 2016). They have attributed this effect to a higher volatility and/or ionization of ^{207}Pb atoms due to their non-zero nuclear spin resulting from an odd number of neutrons and an even number of protons. The magnitude of the offset is dependent on filament temperature range during the analyses, silica gel properties and the degree to which the sample is exhausted during the analyses. In the worst-case scenarios, there may be an offset of more than 0.1% of the ^{207}Pb/^{206}Pb ratio relative to the even-even isotope ratios but care in working to minimize the effects by using well-characterized silica gel and not running samples to exhaustion reduces the offset to under 0.03%. The effect can be further reduced when considering how to apply mass fractionation correction using the even–odd ^{202}Pb–^{205}Pb mixed tracer. Theoretically, the even–odd tracer is better suited to correct for unknown odd–even ^{207}Pb/^{206}Pb ratios than for even-even ^{204}Pb/^{206}Pb ratios, a situation well suited to chronology since the ^{207}Pb/^{206}Pb ratio is the more critical ratio for calculating an age. However, the ^{202}Pb–^{205}Pb ratio of the spike has been calibrated against the even-even ^{208}Pb/^{206}Pb ratio of 2.1667 for NBS981 in at least two laboratories using this method (Amelin and Davis, 2006; Connelly et al., 2012). Without a correction for the enhanced evaporation/ionization of ^{205}Pb, the resulting calibration of the ^{202}Pb/^{205}Pb ratio of the tracer would be too low. Using this value to correct for even–even ratios will return the correct values whereas the application to even–odd ratios will contain an offset equivalent to the degree of enhanced ^{205}Pb over ^{202}Pb. A mass independent enhancement of 0.01% of the calibrated ^{205}Pb/^{202}Pb ratio will result in commensurately false enhancements of all measured ^{207}Pb/^{206}Pb ratios that will translate into offsets in the ^{207}Pb/^{206}Pb ages of 0.15 Myr older than the actual ages. It must be reiterated that this effect is only observed for TIMS analyses using silica gel as a loading medium. As such, it recommends extreme caution when comparing ages from the two methods or even two TIMS-based laboratories that have calibrated their tracer solutions differently. Finally, the possibility of inter-laboratory biases fully precludes third party users from "cherry-picking" points from different studies to calculate an age that may better support one model or another. On the other hand, it should be clear that the comparison of Pb–Pb ages generated within one laboratory or between laboratories using the same methods and tracer solutions will be a more reliable means of establishing accurate relative ages. An alternative option will be to use appropriate standard solutions that replicate the Pb isotopic composition of fractions used to define meteoritic isochrons – this future option is discussed in more detail below.

7. AGE UNCERTAINTIES AND ERROR CORRELATION

The assigned uncertainty for an age calculated in the inverse Pb space corresponds to the precision of the *y*-axis intercept in ^{204}Pb/^{206}Pb vs ^{207}Pb/^{206}Pb plot. The uncertainties on this calculated ratio depends on the proximity of the most radiogenic points to the *y*-intercept, the spread of analyses to constrain a statistically-acceptable line (except for samples with analyses of pure radiogenic Pb), the magnitude of the errors on each point and the shape of the error ellipse that expresses both the correlation of errors for the two axes and the uncertainty caused by the common Pb correction. In inverse Pb–Pb space, the error correlation between the two axes of (^{207}Pb/^{206}Pb) vs (^{204}Pb/^{206}Pb) is small given that the denominator ^{206}Pb common to both axes is the most abundant isotope of the three measured. The laboratory Pb blank correction can dominate the uncertainties on the analyses of small amounts of Pb relative to the total blank, resulting in an uncertainty on individual analyses that are represented by ellipses with the long axes oriented towards the Pb isotopic composition of the Pb blank (Fig. 8). The size of the ellipse resulting from the blank correction depends on the relative amounts of sample and blank Pb and the assigned uncertainty on the amount of blank, a value that is typically estimated to be ±50% or more. Estimating the total amount of Pb blank added and its isotopic composition is based on repeated determinations of the Pb recovered from the full procedure. The size and shape of the error ellipses play an important role in the final uncertainty of a calculated age. The alignment of error ellipses with long axes pointing towards the Pb isotopic composition of modern terrestrial Pb and sub-parallel to isochrons on inverse Pb–Pb plots results in more tightly-constrained isochrons and, therefore, intercepts and ages.

A best case scenario with highly-radiogenic points and an array defined by a spread of points all with standard analytical errors on individual ratios will typically yield an uncertainty on the final calculated age of ~±0.2 Myr (e.g. Connelly et al., 2012). An additional uncertainty of ~±0.1 Myr for the analytical precision of the U isotopic precision must be added in quadrature, for a total uncertainty of ~± 0.25 Myr for a U-corrected Pb–Pb absolute age. Errors significantly lower than these values for materials with limited amounts of Pb will require the development

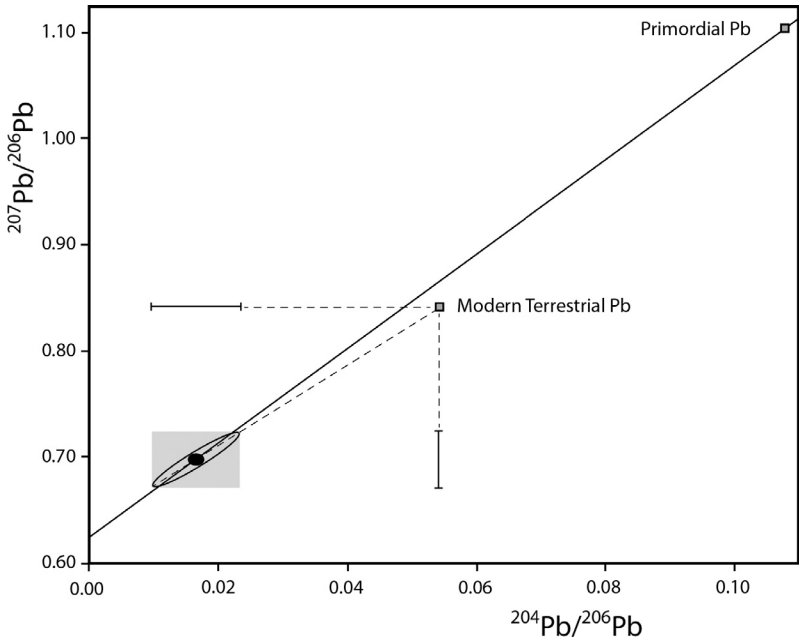

Fig. 8. In this hypothetical example, the small black ellipse corresponds to the uncertainties related to the measurement error from the mass spectrometer that are only weakly correlated. The surrounding larger open ellipse reflects the uncertainty on the amount of laboratory Pb blank that was removed from the sample. This generates larger errors for small samples on both the $^{207}Pb/^{206}Pb$ and $^{204}Pb/^{206}Pb$ ratios, as shown by the lines with ticks on either ends. Given that the blank corrected composition must lie along the line connecting the centroid of the analyses and modern terrestrial Pb, the uncertainty on the blank subtraction results in an error ellipse with the long axis pointing towards the assumed isotopic composition of the Pb blank and the short axes corresponding to the magnitude of the measurement error ellipse (black ellipse). For samples where modern terrestrial Pb lies below the isochrons, an over-subtraction of Pb blank will result in a point above their corresponding isochron whereas subtracting too little Pb will result in points below the isochron.

of more advanced instrumentation to precisely analyze small amounts of Pb and a corresponding improvement in the laboratory blank.

8. REVIEW OF CURRENT EARLY SOLAR SYSTEM CHRONOLOGY

The ultimate goal of chronology as applied to meteorites is to constrain the timing of objects and processes from the early Solar System as precisely as possible with ages that are accurate within their stated uncertainties. A number of issues may complicate this seemingly straight forward goal including: (1) samples that yield data complicated by secondary processes and that are difficult or impossible to interpret, (2) the use of different radiogenic systems that may have different closure temperatures, (3) the use of radiogenic systems that are underpinned by assumptions that may not be correct, and (4) the comparison of ages based on the same radiogenic system but produced in different laboratories using non-standardized methods. This section reviews the chronology of critical samples and processes while evaluating the degree of confidence we can place on the various ages cited.

8.1. The Solar Systems oldest solids – calcium aluminum inclusions

There has been a long-standing debate about the true age of CAIs. Amelin et al. (2002) provided the first high-precision age estimate for a single CAI of 4567.17 $\pm$ 0.70 Ma using different fragments, grain sizes and acid leaching steps. This work was accomplished using a TIMS instrument prior to the development of a mixed $^{202}Pb/^{205}Pb$ tracer so that the uncertainty on the instrumental mass fractionation represents the largest analytical uncertainty. More problematic, the $^{238}U/^{235}U$ ratio of the inclusion was assumed at that time to be 137.88. It is now known that this ratio can vary in CAIs up to 30 ε units corresponding to an age correction of 5 Myr (Brennecka et al., 2010) and up to 590 ε units in one anomalous CAI (Tissot et al., 2016). A second commonly-cited Pb–Pb age of 4568.2 $+0.2/-0.4$ Ma for a single CAI was published by Bouvier and Wadhwa (2010), an age that is slightly older outside of the stated errors of that from Amelin et al. (2002). This age was produced by MC-ICP-MS using Tl to internally correct for instrumental mass fractionation and it reflects a $^{238}U/^{235}U$ ratio based on a presumed correlation between Nd/U and the U isotopic composition that was inferred by Brennecka et al. (2010). This was later shown to be an unreliable indicator of the U isotopic composition (Amelin et al., 2010 and Connelly et al., 2012) such that the $^{238}U/^{235}U$ ratio of this CAI is not known and this age should also be disregarded. The first U-corrected Pb–Pb age produced for a single CAI was published by Amelin et al. (2010) for the large Allende CAI labeled SJ-100. They determined an age of 4567.18 $\pm$ 0.50 Ma, where the error reflects all analytical uncertainties combined in quadrature including that for the measured U isotopic composition.

While this age overlaps the age of Amelin et al. (2002), this must be fortuitous given that U isotopic composition was unconstrained for the earlier age. The most recently published ages of single CAIs was reported by Connelly et al. (2012), who reported three U-corrected ages for CAIs with diverse textures from the CV chondrite Efremovka. Of these three ages, the data for the fine-grained CAI 22E reviewed above represents the best case scenario where 12 of 20 washes and dissolution steps (and all the advanced dissolution steps except the residue) define a well-correlated isochron with an age of 4567.35 ± 0.28 (MSWD = 0.91). Furthermore, the regression projects back to the accepted Pb isotopic composition of the Solar System, consistent with such a reservoir serving as the non-radiogenic Pb in this sample (see also below). The pooled ages of these three U-corrected Pb–Pb ages with that of Amelin et al. (2010), representing all published U-corrected Pb–Pb ages, derives a best estimate of CAIs of 4567.30 ± 0.16 Ma (Fig. 9). Given that it is widely accepted that CAIs represent the oldest objects formed in our in our Solar System (see review by MacPherson, 2014), this age may also be taken to represent the current best estimate of the age of our Sun and the establishment of the protoplanetary disk.

8.2. Intial Pb in CAIs

As high temperature condensates that lack primary volatile elements, CAIs are expected to contain elevated abundances of refractory U and be essentially free of initial Pb. However, all four published U-corrected Pb–Pb ages for CAIs are based on regressed lines that naturally project through primordial Pb, indicating that a non-radiogenic Pb component exists in these analyses. The fact that all four isochrons project well above the field for modern terrestrial Pb confirms that this non-radiogenic component is not field or laboratory contamination. This component is most compatible with Pb occurring in the matrix that will be present in high concentrations (~2500 ppb Pb) and with an unradiogenic isotopic composition resulting from a low μ-value of ~0.2. Whether this Pb was included in the analyses by virtue of Pb having transferred from matrix to the CAI or a small amount of matrix that was not removed during sample preparation, the ages remain robust by virtue of the isochrons being based on two components, namely pure radiogenic Pb from the CAI and Pb from the matrix that has an isotopic composition very close to primordial Pb. Since the unradiogenic matrix Pb represents a distinct end-member reservoir regardless of how it was incorporated into the analyses, the regression can correctly identify the radiogenic Pb composition that corresponds to the y-axis of the inverse Pb–Pb diagram.

8.3. The Pb–Pb ages of chondrules

Chondrules form from primitive dust that has been heated above its melting temperature and rapidly cooled (see review by Scott and Krot, 2014). "Nebular chondrules" are taken here as chondrules that formed within the protoplanetary disk before the dust and gas cleared. A second group of chondrules apparently formed by planetary collisions (Krot et al., 2005). The range of textures is controlled in part by the peak temperatures achieved relative to the liquidus temperature of the individual chondrule. Whereas U concentrations are mainly inherited from the primitive dust, the amount of volatile elements, including Pb, appears to reflect the number and extent of thermal processing events resulting in μ-values that range from the 20's to 100's (Connelly et al., 2012; Bollard, 2016). Initial attempts to date nebular chondrules pooled a number of smaller chondrules that resulted in ages that were 4563.66 ± 0.63 (Amelin et al., 2002) and 4564.32 ± 0.81 Ma (Connelly and Bizzarro, 2009; both ages adjusted for a U isotopic composition of 137.786). These ages can only reflect the average age of the chondrules pooled for these studies. Large chondrules formed by a planetesimal collision have

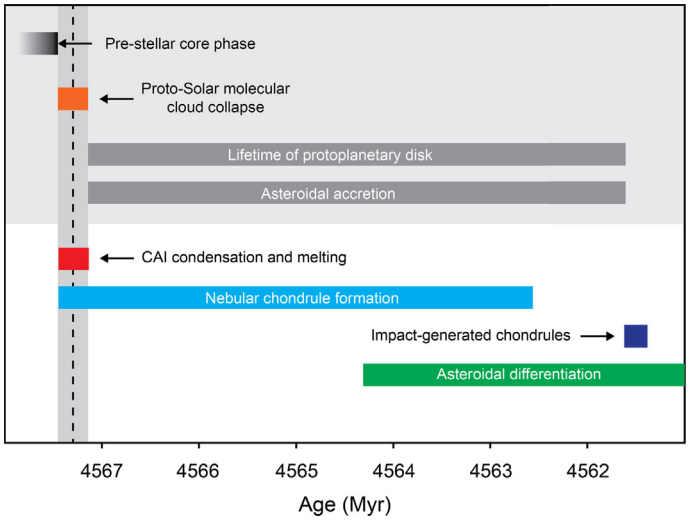

Fig. 9. Summary diagram of the chronology of the early Solar System based on Pb–Pb geochronology.

been dated using individual inclusions with an average age of 4562.49 ± 0.21 Ma (Fig. 9; using an U isotopic composition of 137.786; Bollard et al., 2015).

As the only published report of U-corrected Pb–Pb ages for individual nebular chondrules, Connelly et al. (2012) reported a range of ages for five chondrules from 4567.32 ± 0.42 Ma to 4564.71 ± 0.30 Ma. The isochrons for all five chondrules project back to an initial isotopic composition that is close to the presumed primordial isotopic composition of the Solar System, but comprising both less and more radiogenic values relative to Canyon Diablo troilite Pb (Tatsumoto et al., 1973). This was inferred by Connelly et al. (2012) to indicate that the Pb isotopic composition of the Solar System was less radiogenic than that for Canyon Diablo troilite and that the different chondrules reflect a progressive evolution of radiogenic Pb in their respective precursors. In all cases, the isochrons projected well above the field for modern terrestrial Pb indicating that this was not the source of non-radiogenic Pb in the fractions used to define the isochrons. This study concluded that the ages derived for the five well-defined isochrons with sensible extrapolations to initial Pb compositions represent the age of the last crystallization of these chondrules. They ranged in age from the oldest chondrule that overlaps the brief formation age of CAIs to 2.6 Myr after t_0, such that the first chondrules formed contemporaneously with CAIs and that nebular chondrules forming processes lasted for at least 2.6 Myr. A subsequent study of individual chondrules has confirmed the oldest ages of chondrules and extends the age range of nebular chondrules formation to 3.6 Myr after t_0 (Fig. 9; Bollard, 2016).

8.4. ^{26}Al–^{26}Mg systematics of chondrules

A number of studies report a ~1.0–1.5 Myr gap in ^{26}Al–^{26}Mg ages for chondrules relative to CAIs, a result that inherently presumes the ^{26}Al/^{27}Al ratio was homogeneously distributed in the protoplanetary disk throughout it's lifetime (e.g. Villeneuve et al. (2009) and Kita et al. (2013) and references therein). This assumption was challenged by Larsen et al. (2011) and Schiller et al. (2015) who showed that some differentiated bodies inherited up to 80% less ^{26}Al relative to ^{27}Al than that predicted by CAIs, which is thought to reflect a reduced initial ^{26}Al/^{27}Al ratio of disk solids at the time of CAI formation. A major obstacle in evaluating the robustness of the ^{26}Al–^{26}Mg ages relative to the Pb–Pb ages for chondrules lies in the dearth of ages from both systems for individual chondrules. This has been remedied by a study where both Pb–Pb and ^{26}Al–^{26}Mg ages are assessed for single chondrules from the CV chondrite Allende and the ordinary chondrite NWA 5697 (Bollard, 2016). The results of this study shows a systematic offset between the Pb–Pb and ^{26}Al–^{26}Mg ages defined by internal isochrons, which the author interprets to reflect a lower abundance of ^{26}Al in the chondrule forming region of the protoplanetary disk than in the CAI forming region at t_0. As such, we conclude here that the ^{26}Al/^{27}Al ratios of chondrules cannot be directly compared to that of CAIs for the sake of determining their relative ages.

8.5. Hf–W chronology of chondrules

Budde et al. (2016) noted that the ~3 Myr span of chondrule formation documented by Connelly et al. (2012) is inconsistent with presumed chemical and isotopic complementary between chondrules and matrix that supports models of local and/or brief chondrule formation (i.e. Palme et al., 2015; Ebel et al., 2016). They inferred that the Pb–Pb ages reflect late stage parent body alteration without providing any specific mechanism to explain isochrons as old as CAIs. Instead, they suggested that the short-lived ^{182}Hf–^{182}W decay system (half-life = 8.9 Myr) applied to 100's or 1000's of chondrules as well as matrix and bulk samples is a better method of obtaining the true age range of chondrules. A similar approach was used by Becker et al. (2015). Using matrix, bulk samples and bulk chondrules to define ^{182}Hf–^{182}W isochrons requires independent evidence for a single, closed-system Hf–W fractionation event affecting the matrix and chondrules to fulfill the basic requirement of a meaningful isochron.

They used arguments for complementarity between chondrules and matrix, including their own ^{183}W data, to infer a brief formation interval for chondrules and their immediate accretion to form chondrites with cogenetic matrix. Invoking this model to infer coeval fractionation of Hf and W between chondrules and matrix, Budde et al. (2016) used these entities and mixtures of them to define a Hf–W array that corresponds to an age of 2.2 ± 0.8 Myr after the formation of CAIs that they accept as the time window of chondrule formation. This overlaps the result of Becker et al. (2015) who defined a chrondrule formation window of −0.9 ± 2.8 Myr relative to the formation age of CAIs. However, a recent Mg and ^{54}Cr isotope study of individual CV chondrules does not support the required complementarity between matrix and chondrules (Olsen et al., 2016). Furthermore, linearity of large multi-chondrule fractions in Hf–W space is predicted if the age distributions of the various populations are similar, even if they are not coeval. In this case, their age would approximate the average age of chondrules if the Hf/W ratio of the matrix is close to the composition of the bulk Solar System. Finally, we note that Pb isotopic measurements on bulk CV chondrule samples also derives an average age for chondrule formation of 2.85 ± 0.45 Myr after CAI formation (Connelly et al., 2008; re-calculated using ^{238}U/^{235}U of 137.786, Connelly et al., 2012), which overlaps their estimated Hf–W average age. This may indicate that both systems remained closed in each chondrule after their respective final nebular heating event and, therefore, both are capable of returning average age information about chondrule formation, even in an aqueously-altered and metamorphosed meteorite such as Allende.

8.6. Ages of differentiated meteorites

The Pb–Pb method requires a significant enhancement of U over Pb relative to their Solar abundances to produce sufficiently radiogenic Pb isotopic compositions that will

return useful ages with low uncertainties. Whereas the high temperature processes that form CAIs and chondrules ensure elevated μ-values, it is less certain how processes leading to the formation of samples from differentiated bodies will affect the U/Pb ratio. As such, the chances of successfully dating an individual differentiated meteorite will depend on the U/Pb ratio of the planetesimal's precursor material and whether there was any process or processes that elevated the μ-value of the parental magma or the derivative meteorites. The suite of volatile-depleted angrite meteorites serve as the best example of differentiated meteorites that are readily amenable to Pb–Pb dating due to their very high μ-values. Several samples yield acid-leached mineral separates that have only radiogenic Pb so that a Pb–Pb age can be determined directly from this composition (i.e. Amelin, 2008a,b; Connelly et al., 2008). Diogenites and samples from Mars represent the other end of the spectrum where their parent bodies, parental magmas and the final differentiated meteorites have much lower μ-values. Graphically expressed, the latter cases result in long extrapolations to the y-axis on an inverse Pb–Pb plot such that their isotopic compositions of the radiogenic Pb, and, therefore, their Pb–Pb ages, are poorly constrained.

Recent models of planetesimal formation by streaming instabilities leading to efficient chondrule accretion predict that planetesimals will effectively begin forming contemporaneously with the first appearance of chondrules (Johansen et al., 2015). As such, the documentation of the earliest chondrules having formed coevally with CAIs predicts that planetesimals began to form very early in the lifetime of the protoplanetary disk. Whereas planetesimal formation cannot itself be directly dated, the onset of the process can be at least constrained by the age of the oldest differentiated meteorite. The coarse-grained angrite NWA 1670 was processed using the stepwise dissolution procedure and analyzed using a TIMS (Schiller et al., 2015) to derive a Pb–Pb age of 4564.39 ± 0.24 Ma. That this sample represents at least the partial solidification of a planetesimal mantle by this time requires that planetesimal formation, differentiation and magmatism was well underway within ~3.0 Myr after CAI formation (Fig. 9). The Pb–Pb ages of the youngest nebular chondrules indicates that they were still forming by this time, confirming that some chondrites must have accreted after the differentiated bodies were already formed and providing permissive evidence for chondrite accretion to crusts on already differentiated bodies (Elkins-Tanton et al., 2011).

8.7. Using differentiated meteorites to assess the ^{26}Al–^{26}Mg "Chronometer

A common approach to test for homogeneity of ^{26}Al relative to ^{27}Al in the protoplanetary disk lies in determining the ages of unequilibrated differentiated meteorites relative to CAIs using both the Pb–Pb and ^{26}Al–^{26}Mg system to check whether there is concordancy between the two systems. An early review by Nyquist et al. (2009) of data available at that time concluded that relative ages for differentiated bodies calculated by the ^{26}Al–^{26}Mg system did not match those determined from Pb–Pb ages. This conclusion remains valid even with a shift of 1 Myr to a younger age for the angrites due to the redefined U isotopic composition. Subsequent individual tests have both agreed and disagreed with this assessment. Schiller et al. (2015) showed that the abundance of ^{26}Al relative to ^{27}Al for the angrite parent body was 4 times lower at t_0 than the canonical value defined by CAIs. Bouvier et al. (2011) concluded that ungrouped basaltic meteorite NWA 2976 returned Pb–Pb and ^{26}Al–^{26}Mg ages relative to CAIs that demonstrated homogeneity of ^{26}Al in the protoplanetary disk. However, they used a Pb–Pb age for CAIs without specific knowledge of its ^{238}U/^{235}U ratio, which may account for their age being 0.9 Myr older than the 4567.30 ± 0.16 Ma averaged age of four CAIs reported by Connelly et al. (2012) and Amelin et al. (2010). Furthermore, they used a measured ^{238}U/^{235}U ratio to calculate the Pb–Pb age for NWA 2976 that was ~2.5 ε lower than that measured for the same sample by Connelly et al. (2012) and for the recommended Solar System value by four subsequent independent studies (Connelly et al., 2012; Brennecka and Wadhwa, 2012; Brennecka et al., 2015; Goldmann et al., 2015). Using the CAI age of Connelly et al. (2012) and adjusting the Pb–Pb age of NWA 2976 for the ~2.5 ε offset in the U isotopic composition translates to an initial abundance of ^{26}Al relative to ^{27}Al for the parent body of NWA 2976 that is 2.8 times lower than the CAI canonical value. More recently, Larsen et al. (2016) used high precision Mg isotope measurements for differentiated and undifferentiated meteorites to argue for reduced abundances of initial ^{26}Al relative to ^{27}Al at t_0 that varies with heliocentric distance from values of 1.6×10^{-5} in the inner Solar System to 2.8×10^{-5} in the outer Solar System.

9. FUTURE WORK

There is now abundant evidence based on the ^{26}Al–^{26}Mg decay system that CAIs formed in a single, brief interval that may have spanned less than 4000 years (i.e. Larsen et al., 2011). There is no clear evidence from the ^{26}Al–^{26}Mg decay system that CAIs formed at different times episodically or continuously over a longer time frame. The absolute age for this event appears to be best represented by the weighted means average Pb–Pb age of 4567.30 ± 0.16 Ma for four CAIs from 2 CV chondrites dated in two independent laboratories. The Pb isotopic compositions of these four inclusions were measured by TIMS using separate equal atom ^{202}Pb–^{205}Pb tracer solutions that were independently calibrated against NIST981 with a ^{208}Pb/^{206}Pb ratio of 2.1677. Whether this age is accurate within the stated 0.16 Myr uncertainties depends on the respective calibrations of the ^{202}Pb–^{205}Pb tracers and the degree of any mass independent fractionation that may arise from the odd–even effect of the ^{207}Pb/^{206}Pb radiogenic ratio.

It should be noted that the exact absolute age of CAIs and, by inference, the Solar System is not critical to any important scientific question. Our understanding of how the Solar System formed only requires confidence in the relative ages of CAIs with respect to other early Solar System objects, especially chondrules and events on differentiated parent bodies. Any claims of an older age than the

TIMS-based age of 4567.30 ± 0.16 Ma raise several possibilities. First, there could have been multiple epochs of primary CAI formation such that both ages reliably record the distinct ages of different CAI populations. At present, the co-linearity of ^{26}Al–^{26}Mg data for a number of CAIs from CV chondrites by several laboratories offers the strongest support for a single, brief CAI forming event, at least for CAIs from CV chondrites. Secondly, all CAIs may have formed in a single event but a subset was thermally affected yielding younger ages that reflect a secondary metamorphic event. The reproducibility of four ages for CAIs from CV chondrites (one of which exhibits a fine-grained texture and mineralogy consistent with a primary condensate) with individually-measured unique $^{238}U/^{235}U$ ratios, including two CAIs that fall on the canonical Al–Mg array of Larsen et al. (2011) suggests that the age of 4567.30 ± 0.16 Ma represents the primary formation age of CAIs from CV chondrites. Any CAIs from this group that were affected by secondary processing would necessarily yield either younger ages or be only partially reset such that no age information could be ascertained. Thirdly, it may reflect an inter-laboratory bias reflecting an inability to reproducibly measure Pb and/or U isotope ratios with accuracies within the stated uncertainties by either or both methods employed. We conclude that any claims of an older or younger epoch of primary CAI formation in CV chondrites may reflect inter-laboratory biases and that this possibility requires cooperative efforts to verify or disprove.

The prospect of a Pb or U isotopic measurement bias between two laboratories using different methods and types of instruments (MC-ICP-MS vs TIMS) has not been rigorously tested. All laboratories routinely run pure Pb and U solutions to confirm that each instrument is capable of determining the accepted values for a pure solution with a known isotopic composition. It is more difficult to determine whether ideal fractionation laws apply to real samples that may have a minor component of matrix elements remaining after the chemical purification of Pb and U.

We propose two methods to validate direct inter-laboratory comparisons of Pb–Pb ages in future work. The first involves the analyses of a series of five pure Pb solutions that define an array in $^{204}Pb/^{206}Pb$ vs $^{207}Pb/^{206}Pb$ space comparable to that obtained for radiogenic meteorite samples. These solutions were produced by creating end-member synthetic solutions comparable to primordial Pb and a highly-radiogenic solution with a $^{207}Pb/^{206}Pb$ ratio corresponding to an age of ~4557 Ma. These concentrated end-member solutions were mixed together to make 4 intervening isotopic compositions. These four mixed solutions and the end-member radiogenic solution comprise the set of five standard solutions available for distribution through the EarlyTime initiative (Connelly and Condon, 2014). A second method to validate inter-laboratory methods lies in the CBa chondrite Gujba that contains large (cm sized) chondrules that are proposed to have formed simultaneously at 4562.49 ± 0.21 (Bollard et al., 2015). This meteorite is abundant and widely available with large, easily-separated chondrules that have yielded linear arrays and, therefore, ages in two different laboratories (Krot et al., 2005; Bollard et al., 2015). A single piece of the meteorite could be mined for chondrule fragments for distribution to participating laboratories.

ACKNOWLEDGEMENTS

We thank journal referees Fernando Corfu, Robert Zartman and an anonymous reviewer along with the handling editor Yuri Amelin for their constructive comments that improved the paper. Funding for this project was provided by a grant from the Danish Agency for Science, Technology and Innovation (grant number 12-125692) to JNC as well as grants from the Danish National Research Foundation (grant number DNRF97) and from the European Research Council (ERC Consolidator grant agreement 616027-STARDUST2ASTEROIDS) to MB.

REFERENCES

Amelin Y. (2008a) The U–Pb systematics of angrite Sahara 99555. *Geochim. Cosmochim. Acta* **72**, 4874–4885.

Amelin Y. (2008b) U–Pb ages of angrites. *Geochim. Cosmochim. Acta* **72**, 221–232.

Amelin Y. and Davis W. J. (2006) Isotopic analysis of lead in sub-nanogram quantities by TIMS using ^{202}Pb–^{205}Pb spike: application to geochronology and cosmochronology. *Geochim. Cosmochim. Acta* **70**, A14.

Amelin Y. and Huyskens M. (2013) Performance of Pb Multi Ion Counting Array in Triton Plus TIMS. Goldschmidt Conference Abstracts, A586.

Amelin Y., Krot A. N., Hutcheon I. D. and Ulyanov A. A. (2002) Lead isotopic ages of chondrules and calcium–aluminum-rich inclusions. *Science* **297**, 1678–1683.

Amelin Y., Davis D. W. and Davis W. J. (2005) Decoupled Fractionation of Even-and Odd-mass Isotopes of Pb in TIMS. Goldschmidt Conference Abstracts, A215.

Amelin Y., Connelly J., Zartman R. E., Chen J. H., Göpel C. and Neymark L. A. (2009) Modern U–Pb chronometry of meteorites: advancing to higher time resolution reveals new problems. *Geochim. Cosmochim. Acta* **73**, 5212–5223.

Amelin Y., Kaltenbach A., Iizuka T., Stirling C. H., Ireland T. R., Petaev M. and Jacobsen S. B. (2010) U–Pb chronology of the Solar System's oldest solids with variable $^{238}U/^{235}U$. *Earth Planet. Sci. Lett.* **300**, 343–350.

Amelin Y., Yin Q. -Z., Koefoed P. and Merle R. (2016) Fractionation of Radiogenic Pb Isotopes Induced by Acid Leaching: A Pervasive Phenomenon in Pb-isotopic Dating of Meteorites. Goldschmidt Conference Abstracts, A57.

Baker J., Peate D., Waight T. and Meyzen C. (2004) Pb isotopic analysis of standards and samples using a ^{207}Pb–^{204}Pb double spike and thallium to correct for mass bias with a double-focusing MC-ICP-MS. *Chem. Geol.* **211**, 275–303.

Becker M., Hezel D. C., Schulz T., Elfers B.-M. and Münker C. (2015) Formation timescales of CV chondrites from component specific Hf–W systematics. *Earth Planet. Sci. Lett.* **432**, 472–482.

Bollard J. (2016) Early Disk Dynamics Inferred from Isotope Systematics of Individual Chondrules – Absolute Chronology of the Solar Protoplanetary Disk Revisited. (Ph.D. thesis). University of Copenhagen, Copenhagen, Denmark. p. 184.

Bollard J., Connelly J. N. and Bizzarro M. (2015) Pb–Pb dating of individual chondrules from the CBa chondrite Gujba: assessment of the impact plume formation model. *Meteorit. Planet. Sci.* **50**, 1197–1216.

Borg L. E., Connelly J. N., Boyet M. and Carlson R. W. (2011) Chronological evidence that the Moon is either young or did not have a global magma ocean. *Nature* **477**, 70–72.

Bouvier A. and Wadhwa M. (2010) The age of the Solar System redefined by the oldest Pb–Pb age of a meteoritic inclusion. *Nat. Geosci.* **3**, 637–641.

Bouvier A., Spivak-Birndorf L. J., Brennecka G. A. and Wadhwa M. (2011) New constraints on early Solar System chronology from Al–Mg and U–Pb isotope systematics in the unique basaltic achondrite Northwest Africa 2976. *Geochim. Cosmochim. Acta* **75**, 5310–5323.

Brennecka G. A. and Wadhwa M. (2012) Uranium isotope compositions of the basaltic angrite meteorites and the chorological implications for the early Solar System. *Proc. Natl. Acad. Sci.* **109**, 9299–9303.

Brennecka G. A., Weyer S., Wadhwa M., Janney P. E., Zipfel J. and Anbar A. D. (2010) $^{238}U/^{235}U$ variations in meteorites: extant ^{247}Cm and implications for Pb–Pb dating. *Science* **327**, 449–451.

Brennecka G. A., Budde G. and Kleine T. (2015) Uranium isotopic composition and absolute ages of Allende chondrules. *Meteorit. Planet. Sci.* **50**, 1995–2002.

Budde G., Kleine T., Kruijer T. S., Burkhardt C. and Metzler K. (2016) Tungsten isotopic constraints on the age and origin of chondrules. *Proc. Natl. Acad. Sci.* **113**, 2886–2891.

Connelly J. N. and Bizzarro M. (2009) Pb–Pb dating of chondrules from CV chondrites by progressive dissolution. *Chem. Geol.* **259**, 143–151.

Connelly J. N. and Bizzarro M. (2016) Lead isotope evidence for a young formation age of the Earth-Moon system. *Earth Planet. Sci. Lett.* **452**, 36–42.

Connelly J. N. and Condon D. J. (2014) Interlaboratory Calibration of Mass Spectrometric Methods used for Pb–Pb Dating of Meteorites under the Auspices of the Early Time Initiative. Goldschmidt Conference Abstracts, A448.

Connelly J. N., Bizzarro M., Thrane K. and Baker J. A. (2008a) The Pb–Pb age of Angrite SAH99555 revisited. *Geochim. Cosmochim. Acta* **72**, 4813–4824.

Connelly J. N., Amelin Y., Krot A. N. and Bizzarro M. (2008b) Chronology of the Solar System's oldest solids. *Astrophys. J.* **675**, L121–L124.

Connelly J. N., Bizzarro M., Krot A. N., Nordlund Å., Wielandt D. and Ivanova M. A. (2012) The absolute chronology and thermal processing of solids in the solar protoplanetary disk. *Science* **338**, 651–655.

Doucelance R. and Manhès G. (2001) Reevaluation of precise lead isotope measurements by thermal ionization mass spectrometry: comparison with determinations by plasma source mass spectrometry. *Chem. Geol.* **176**, 361–377.

Ebel D. S., Brunner C., Konrad K., Leftwich K., Erb I., Lu M., Rodriguez H., Crapster-Pregont E. J., Friedrich J. M. and Weisberg M. K. (2016) Abundance, major element composition and size of components and matrix in CV, CO and Acfer 094 chondrites. *Geochim. Cosmochim. Acta* **172**, 322–356.

Elkins-Tanton L. T., Weiss B. P. and Zuber M. T. (2011) Chondrites as samples of differentiated planetesimals. *Earth Planet. Sci. Lett.* **305**, 1–10.

Goldmann A., Brennecka G., Noordmann J., Weyer S. and Wadhwa M. (2015) The uranium isotopic composition of the Earth and the Solar System. *Geochim. Cosmochim. Acta* **148**, 145–158.

Jaffey A. H., Flynn K. F., Glendinin L. E., Bentley W. C. and Essling A. M. (1971) Precision measurement of Half-Lives and Specific Activities of ^{235}U and ^{238}U. *Phys. Rev. C* **4**, 1889–1906.

Johansen A., Low M.-M. M., Lacerda P. and Bizzarro M. (2015) Growth of asteroids, planetary embryos, and Kuiper belt objects by chondrule accretion. *Sci. Adv.* **1**, e1500109.

Kaltenbach A. (2012) *Uranium Isotopic Analyses of Terrestrial and Extraterrestrial Samples*. (Ph.D. thesis). University of Otago, Dunedin, New Zealand. p. 174.

Kamenov G. D., Mueller P. A. and Perfit M. R. (2004) Optimization of mixed Pb–Tl solutions for high precision isotopic analyses by MC-ICP-MS. *J. Anal. Atom. Spectrom.* **19**, 1262–1267.

Kita N. T., Yin Q.-Z., MacPherson G. J., Ushikubo T., Jacobsen B., Nagashima K., Kurahashi E., Krot A. N. and Jacobsen S. B. (2013) ^{26}Al–^{26}Mg isotope systematics of the first solids in the early solar system. *Meteorit. Planet. Sci.* **48**, 1383–1400.

Kleine T., Touboul M., Bourdon B., Nimmo F., Mezger K., Palme H., Jacobsen S. B., Yin Q.-Z. and Halliday A. N. (2009) Hf–W chronology of the accretion and early evolution of asteroids and terrestrial planets. *Geochim. Cosmochim. Acta* **73**, 5150–5188.

Krot A. N., Amelin Y., Cassen P. and Meibom A. (2005) Young chondrules in CB chondrites from a giant impact in the early Solar System. *Nature* **436**, 989–992.

Krot A. N., Amelin Y., Bland P., Ciesla F. J., Connelly J., Davis A. M., Huss G. R., Hutcheon I. D., Makide K., Nagashima K., Nyquist L. E., Russell S. S., Scott E. R. D., Thrane K., Yurimoto H. and Yin Q.-Z. (2009) Origin and chronology of chondritic components: a review. *Geochim. Cosmochim. Acta* **73**, 4963–4997.

Larsen K. K., Trinquier A., Paton C., Schiller M., Wielandt D., Ivanova M. A., Connelly J. N., Nordlund Å., Krot A. N. and Bizzarro M. (2011) Evidence for magnesium isotope heterogeneity in the solar protoplanetary disk. *Astrophys. J. Lett.* **735**, L37.

Larsen K. K., Schiller M. and Bizzarro M. (2016) Accretion timescales and style of asteroidal differentiation in an ^{26}Al-poor protoplanetary disk. *Geochim. Cosmochim. Acta* **176**, 295–315.

Le Roux L. J. and Glendenin L. E. (1963) Half-life of ^{232}Th. In: *Proc. National Meeting on Nuclear Energy, Pretoria, South Africa*. pp. 83–94.

Ludwig, K. R. (2003) Isoplot/Ex Version 3.00, A Geochronological Toolkit for Microsoft Excel, Berkeley Geochronology Center Special Publication 4.

MacPherson G. J. (2014) Calcium–aluminum-rich inclusions in chondritic meteorites. In: *Treatise on Geochemistry*, second ed., vol. 1. Meteorites and Cosmochemical Processes. pp. 139–179.

Nyquist L. E., Kleine T., Shih C.-Y. and Reese Y. D. (2009) The distribution of short-lived radioisotopes in the early solar system and the chronology of asteroid accretion, differentiation, and secondary mineralization. *Geochim. Cosmochim. Acta* **73**, 5115–5136.

Olsen M. B., Wielandt D., Schiller M., Van Kooten E. M. M. and Bizzarro M. (2016) Magnesium and ^{54}Cr isotope compositions of carbonaceous chondrite chondrules – insights into early disk processes. *Geochim. Cosmochim. Acta* **191**, 118–138.

Palme H., Hezel D. C. and Ebel D. S. (2015) The origin of chondrules: constraints from matrix composition and matrix-chondrule complementarity. *Earth Planet. Sci. Lett.* **411**, 11–19.

Schiller M., Connelly J. N., Glad A. C., Mikouchi T. and Bizzarro M. (2015) Early accretion of protoplanets inferred from a reduced inner solar system ^{26}Al inventory. *Earth Planet. Sci. Lett.* **420**, 45–54.

Scott E. R. D. and Krot A. N. (2014) Chondrites and their components. In: *Treatise on Geochemistry*, second ed., vol. 1. Meteorites and Cosmochemical Processes. pp. 65–137.

Tatsumoto M., Knight R. J. and Allegre C. J. (1973) Time differences in the formation of meteorites as determined from the ratio of Lead-207 to Lead-206. *Science* **180**, 1279–1283.

Thirlwall M. F. (2000) Inter-laboratory and other errors in Pb isotope analyses investigated using a ^{207}Pb–^{204}Pb double spike. *Chem. Geol.* **163**, 299–322.

Tissot F. L. H., Dauphas N. and Grossman L. (2016) Origin of uranium isotope variations in early solar nebula condensates. *Sci. Adv.* **2**, e1501400.

Van Kooten E. M. M. E., Wielandt D., Schiller M., Nagashima K., Thomen A., Larsen K. K., Olsen M. B., Nordlund Å., Krot A. N. and Bizzarro M. (2016) Isotopic evidence for primordial molecular cloud material in metal-rich carbonaceous chondrites. *Proc. Natl. Acad. Sci.* **113**, 2011–2016.

Villa I. M., Bonardi M. L., De Bièvre P., Holden N. E. and Renne P. R. (2016) IUPAC-IUGS status report on the half-lives of ^{238}U, ^{235}U and ^{234}U. *Geochim. Cosmochim. Acta* **172**, 387–394.

Villeneuve J., Chaussidon M. and Libourel G. (2009) Homogeneous distribution of ^{26}Al in the solar system from the Mg isotopic composition of chondrules. *Science* **325**, 985–988.

White W. M., Albarède F. and Télouk P. (2000) High-precision analysis of Pb isotope ratios by multi-collector ICP-MS. *Chem. Geol.* **167**, 257–270.

Associate editor: Yuri Amelin